Stereoisomerism in Tetrametallic Propeller-like Complexes: a Solid-state and Solution NMR Study on a Tetragallium(III) Derivative

Andrea Cornia,*[a] Adele Mucci,[a] Matteo Briganti,[b] Nathalie Bridonneau,[a],§ Andrea Nava,[a,c] and Alessio Nicolini[a]

[a] Prof. Dr. A. Cornia, Prof. Dr. A. Mucci, Dr. N. Bridonneau, Dr. A. Nava, Dr. A. Nicolini
Dipartimento di Scienze Chimiche e Geologiche & UdR INSTM, Università di Modena e Reggio Emilia, Via G. Campi 103, 41125 Modena, Italy
E-mail: acornia@unimore.it
http://personale.unimore.it/rubrica/dettaglio/acornia

[b] Dr. M. Briganti
Dipartimento di Chimica "U. Schiff" & UdR INSTM, Università di Firenze, Via della Lastruccia 3-13, 50019 Sesto Fiorentino (FI), Italy

[c] Dr. A. Nava
Dipartimento di Scienze Fisiche, Informatiche e Matematiche, Università di Modena e Reggio Emilia, Via G. Campi 213/a, 41125 Modena, Italy

§Current address: Institut de Chimie Moléculaire et des Matériaux d'Orsay, Université Paris-Saclay, CNRS, UMR 8182, 91405 Orsay Cedex, France.

ABSTRACT

Tetragallium(III) complex in $[Ga_4(L^{4\text{-Py}})_2(dpm)_6]\cdot EtOH$, with $H_3L^{4\text{-Py}}$ = 2-(hydroxymethyl)-2-(pyridin-4-yl)propane-1,3-diol and Hdpm = dipivaloylmethane, was investigated as a diamagnetic analogue of tetrametallic, propeller-like single-molecule magnets (SMMs). The chiral molecular structure partitions the six CH_2 protons of each $(L^{4\text{-Py}})^{3-}$ tripodal ligand into two diastereotopic sets. The two signals were clearly detected by ^1H NMR spectroscopy in C_6D_6, proving that Λ and Δ enantiomers interconvert slowly over NMR timescale. Density functional theory calculations provided quantitative agreement with the observed values of chemical shifts and scalar coupling constants across both geminal and long-range interaction pathways. The solid-state structure suggests the occurrence of a lower symmetry stereoisomer (27 mol%), which was clearly identified in the NMR spectra. Since Fe^{3+} forms distinctly more inert complexes than Ga^{3+}, comparable or greater configurational stability is expected for the isostructural Fe^{III}_4, $Fe^{III}_3Cr^{III}$, and $Fe^{III}_3V^{III}$ SMMs, which are difficult to investigate by solution NMR because of the strong paramagnetism.

INTRODUCTION

Tetrametallic complexes with a chiral, propeller-like structure similar to that of Werner's "hexol" salts[1–3] and of some Group 13 alkoxides and aryloxides[4–17] are of great historical significance in coordination chemistry. When the metal ions carry a spin (s), this metal-centred triangular topology is magnetically appealing, as it results in a nonzero spin ground state for both ferro- and antiferromagnetic interactions between the central (M_c) and peripheral (M_p) metal centres. For instance, antiferromagnetic coupling in tetrachromium(III) ($s_c = s_p = 3/2$)[18–20] and tetrairon(III) ($s_c = s_p = 5/2$)[21] species affords $S = 3$ and 5 ground states, respectively. Heteronuclear variants were also accessed.[22–24]

Of special interest are complexes with formula $[Fe^{III}_3M^{III}(L^R)_2(dpm)_6]$, where H_3L^R is tripodal proligand 2-R-2-(hydroxymethyl)propane-1,3-diol (Scheme 1) and Hdpm is dipivaloylmethane. These include Fe^{III}_4,[21,25] chromium-centred $Fe^{III}_3Cr^{III}$ ($s_c = 3/2$, $s_p = 5/2$, $S = 6$)[26–29] and vanadium-centred $Fe^{III}_3V^{III}$ species ($s_c = 1$, $s_p = 5/2$, $S = 13/2$).[30] All these complexes have an easy-axis magnetic anisotropy in the ground state and exhibit directional bistability of the magnetic moment, that is, they behave as single-molecule magnets (SMMs).[25]

One of the most distinctive features of such tetrametallic propellers is their chiral solid-state structure, which was clearly demonstrated by X-ray diffraction. However, retention of a chiral structure in solution was never proved, nor is it known whether the Λ and Δ enantiomers interconvert.

We now provide insight into the solution structure of tetrametallic propellers by investigating their tetragallium(III) analogues. The Ga^{3+} ion is an isosteric diamagnetic substitute for high spin Fe^{3+}, since the two ions have similar ionic radius (0.62 Å and 0.65 Å, respectively, when 6-coordinated).[31] Furthermore, both Ga^{3+} and Fe^{3+} form labile complexes[32] (but see Ref.[33] for an interesting exception). Therefore, gallium(III) analogues are often accessible using the same synthetic techniques as for iron(III) complexes. For instance, $[Ga_4(L^{Ph})_2(dpm)_6]\cdot C_6H_6$ (**1^{Ph}**·C_6H_6) was prepared and used as a crystalline diamagnetic host for $[Fe_4(L^{Ph})_2(dpm)_6]$ (**2^{Ph}**) molecules to study the effect of magnetic dilution on SMM behaviour.[34,35] In a different approach, **1^{Ph}**·Et_2O was doped with Fe^{3+} and Cr^{3+} ions to disclose the origin of magnetic anisotropy in chromium-centred $[Fe_3Cr(L^{Ph})_2(dpm)_6]\cdot Et_2O$.[36] In Ref.[36], a solution of **1^{Ph}**·Et_2O in C_6D_6 was found to exhibit a rich ^{1}H NMR spectrum at 200.13 MHz, but the spectrum was not analyzed in detail.

We herein report the synthesis, crystal structure and solution ^{1}H NMR of a related tetragallium(III) derivative, $[Ga_4(L^{4\text{-}Py})_2(dpm)_6]\cdot$EtOH (**1$^{4\text{-}Py}$**·EtOH). Complex **1$^{4\text{-}Py}$** contains 4-pyridyl substituents on the tripodal ligands (Scheme 1) and is the diamagnetic analogue of $[Fe_4(L^{4\text{-}Py})_2(dpm)_6]$ (**2$^{4\text{-}Py}$**), a SMM

synthon used to assemble supramolecular structures.[37,38] The 1D and 2D ^{1}H NMR spectra of **1$^{4\text{-Py}}$**·EtOH in C_6D_6, collected at 400.13 MHz, prove that Λ and Δ enantiomers are configurationally stable over NMR timescale. In addition, they clearly evidence the occurrence of further stereoisomerism related to the coordination mode of dpm^- ligands bound to Ga_p ions. This type of structural information is unaccessible working directly on $Fe^{III}_3M^{III}$ species due to the paramagnetic broadening of resonance lines.[30,36,39,40]

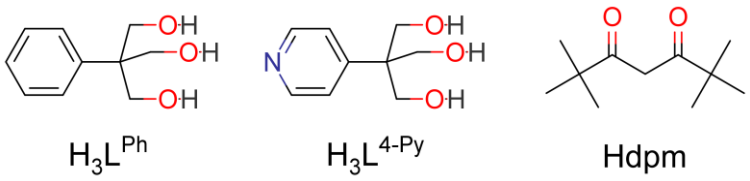

H_3L^{Ph} $H_3L^{4\text{-Py}}$ Hdpm

Scheme 1. Structure of the pro-ligands H_3L^{Ph}, $H_3L^{4\text{-Py}}$ and Hdpm.

RESULTS AND DISCUSSION

Synthesis. Tetrairon(III) propellers with formula $[Fe_4(L^R)_2(dpm)_6]$ are customarily prepared by reacting $[Fe_4(OMe)_6(dpm)_6]$[41,42] with excess tripodal proligand in an appropriate solvent (usually Et_2O).[25] When R = 4-Py, the tripodal proligand is only sparingly soluble in Et_2O and a one pot reaction between $[Fe_2(OEt)_2(dpm)_4]$, $FeCl_3$, $H_3L^{4\text{-Py}}$ and piperidine (pip) in Et_2O/EtOH was utilized to assemble tetrairon(III) complex **2$^{4\text{-Py}}$** in good yield.[38] Since $[Ga_4(OMe)_6(dpm)_6]$ has never been isolated, this alternative synthetic strategy (or variations thereof) is mandatory to access $[Ga_4(L^R)_2(dpm)_6]$ species.[36] Complex **1$^{4\text{-Py}}$** was synthesized in good yield by reacting dimer **4**, $GaCl_3$, $H_3L^{4\text{-Py}}$ and pip in a Et_2O/EtOH solvent mixture, according to Equation (1), and isolated as off-white crystals of the monoethanol solvate.

$$3/2[Ga_2(OMe)_2(dpm)_4]\ (\mathbf{4}) + GaCl_3 + 2H_3L^{4\text{-Py}} + 3pip \longrightarrow [Ga_4(L^{4\text{-Py}})_2(dpm)_6]\ (\mathbf{1^{4\text{-Py}}}) + 3HpipCl + 3MeOH \quad (1)$$

Figure S1 presents the electrospray ionization mass spectrometry (ESI-MS) data obtained by dissolving crystals of **1$^{4\text{-Py}}$**·EtOH in ^{i}PrOH : CH_2Cl_2 (3:1 v/v). The spectrum displays two well resolved signals at *m*/*z* = 1761.7 (100%) and 1745.8 (8%), whose isotopic patterns are consistent with the ionic species $[\mathbf{1^{4\text{-Py}}}+Na]^+$ and $[\mathbf{1^{4\text{-Py}}}+Li]^+$, respectively (sodium and lithium ions are adventitious). A weaker, poorly resolved peak partially overlapping with the signal of $[\mathbf{1^{4\text{-Py}}}+Li]^+$ is also visible at *m*/*z* = 1739.6 (2%); it is assigned to $[\mathbf{1^{4\text{-Py}}}+H]^+$ simply relying on its *m*/*z* value. Mass spectrometry

then provides no evidence that crystals of **1**$^{\mathbf{4\text{-}Py}}$·EtOH contain molecular species compositionally different from **1**$^{\mathbf{4\text{-}Py}}$.

X-ray Crystallography. Compound **1**$^{\mathbf{4\text{-}Py}}$·EtOH is isostructural with its tetrairon(III) analogue **2**$^{\mathbf{4\text{-}Py}}$·2EtOH.[38] As shown in Figure 1, the central ion Ga1 (Ga_c) is coordinated exclusively by the six oxygen donors of the two tripodal $(L^{4\text{-}Py})^{3-}$ ligands, which act as bridges to the three peripheral metals Ga2, Ga3 and Ga3′ (Ga_p). The latter are further coordinated by two dpm^- anions each and all metal ions exhibit a distorted octahedral coordination sphere. A crystallographic twofold axis is directed through Ga1 and Ga2 and relates Ga3 and Ga3′. The molecule consequently has crystallographic C_2 symmetry and the four metal ions are exactly coplanar. As reported in the caption of Figure 1, Ga_c-Ga_p distances are within 0.01 Å from each other and Ga_p-Ga_c-Ga_p angles depart by less than 1° from 120°. Thus, neglecting the 4-pyridyl substituents, the molecule approaches D_3 symmetry quite closely, with an idealized threefold axis normal to the metal plane and three twofold axes along Ga1-Ga2, Ga1-Ga3 and Ga1-Ga3′ directions (Figure 2a). This metal topology is common to many tetragallium(III) compounds.[11,12,14,43–47]

It is interesting to compare the structure of the metal-oxygen core in **2**$^{\mathbf{4\text{-}Py}}$·2EtOH and **1**$^{\mathbf{4\text{-}Py}}$·EtOH, after D_3-symmetry averaging. In the two derivatives, the central metal has a significantly different extent of deviation from octahedral symmetry (O_h).[21,25,48] The twisting angle ϕ between the two opposite triangular faces of the octahedron that lie normal to the threefold axis is 32.7° in **2**$^{\mathbf{4\text{-}Py}}$·2EtOH but 40.0° in **1**$^{\mathbf{4\text{-}Py}}$·EtOH (ϕ = 60° in O_h symmetry). The extent of distortion by trigonal elongation/compression along the threefold axis is also slightly different (θ = 54.2 and 55.4°, respectively, vs. 54.7° in O_h symmetry). Consistent with the smaller trigonal rotation and slight trigonal compression, the pitch γ [21,25,48] of the propeller-like structure decreases from 68.7° in **2**$^{\mathbf{4\text{-}Py}}$·2EtOH to 63.7° in **1**$^{\mathbf{4\text{-}Py}}$·EtOH. Remarkably similar trends were observed in compounds **2**$^{\mathbf{Ph}}$·Et_2O (γ = 68.8°) and **1**$^{\mathbf{Ph}}$·Et_2O (γ = 63.8°),[36] as well as in **2**$^{\mathbf{Ph}}$·C_6H_6 (γ = 68.7°) and **1**$^{\mathbf{Ph}}$·C_6H_6 (γ = 63.7°).[35] Hence, tetragallium(III) derivatives are "weaker propellers" than their tetrairon(III) congeners. These differences are likely related to the smaller ionic radius of gallium(III).[31]

During the refinement of the crystal structure of **1**$^{\mathbf{4\text{-}Py}}$·EtOH we noticed that the first coordination sphere of Ga1 and Ga2 is ordered within experimental resolution. In particular, the β-diketonato ligands bound to Ga2 position their O donor atoms on opposite sides of the molecular plane. The majority of dpm^- ligands bound to Ga3 and Ga3′ also adopt this coordination mode, which is typical for complexes of this family[25] and is hereafter indicated as *propeller*-like (p). However, a fraction (ca. 16%) of dpm^- ligands on Ga3 and Ga3′ display a different, *sandwich*-like (s) coordination mode,

with the two O donors on the same side of the molecular plane. Similar disorder effects were detected in some Fe^{III}_4 [41,42,49] and lanthanoid (Ln)-centred $Fe^{III}_3Ln^{III}$ [50,51] propellers.

We argue that the crystal lattice may comprise three different diastereoisomers: ppp, pps (and its symmetry equivalent psp) and pss. The structure of ppp and pps isomers, which have idealized D_3 and C_2 symmetry, respectively, is compared in Figure 2. Assuming independent occupation probabilities for p- and s-modes on Ga3 and Ga3′, the lattice is expected to contain 70.4% of ppp isomer, 27.0% of pps+psp isomers and 2.6% of pss isomer. Each of these diastereoisomers has two enantiomeric forms which are both present in the centrosymmetric crystal lattice. With reference to the Λ or Δ configuration of the four metal centres, and listing the configuration of the central metal first,[3,24] the ppp isomer exists as Λ(ΔΔΔ) and Δ(ΛΛΛ) enantiomeric pairs (customarily labelled simply as "Λ" and "Δ", respectively), while the pps isomer has Λ(ΔΔΛ) and Δ(ΛΛΔ) enantiomers. All these isomeric forms have exactly the same composition, in agreement with ESI-MS data.

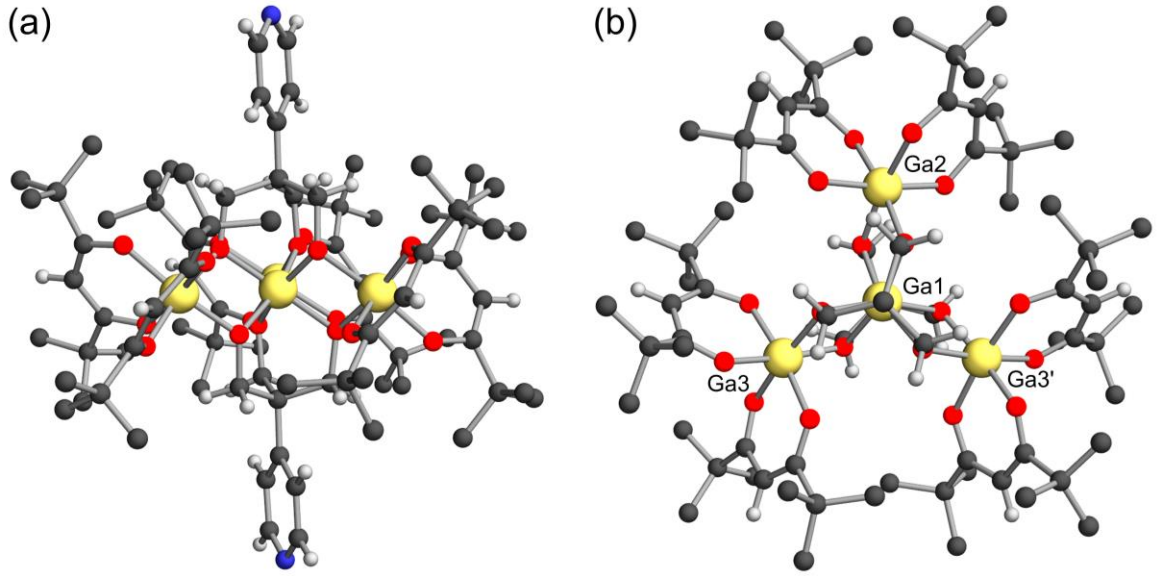

Figure 1. Molecular structure of $\mathbf{1^{4\text{-}Py}}$ in $\mathbf{1^{4\text{-}Py}}$·EtOH, viewed along the twofold axis (a) and normal to the molecular plane (b). For clarity, in (b) the 4-pyridyl groups are not shown. Color code: light yellow = Ga, red = O, blue = N, dark grey = C, light grey = H. Hydrogen atoms of *t*Bu groups and minority components of disordered portions are omitted. Selected interatomic distances and angles: Ga1-Ga2 3.0110(5), Ga1-Ga3 3.0042(3), Ga2-Ga3 5.1993(5), Ga3-Ga3′ 5.2232(6), Ga1-O 1.938-1.954, Ga_p-O 1.941-1.979 Å; Ga3-Ga1-Ga2 119.621(8), Ga3-Ga1-Ga3′ 120.758(15)°.

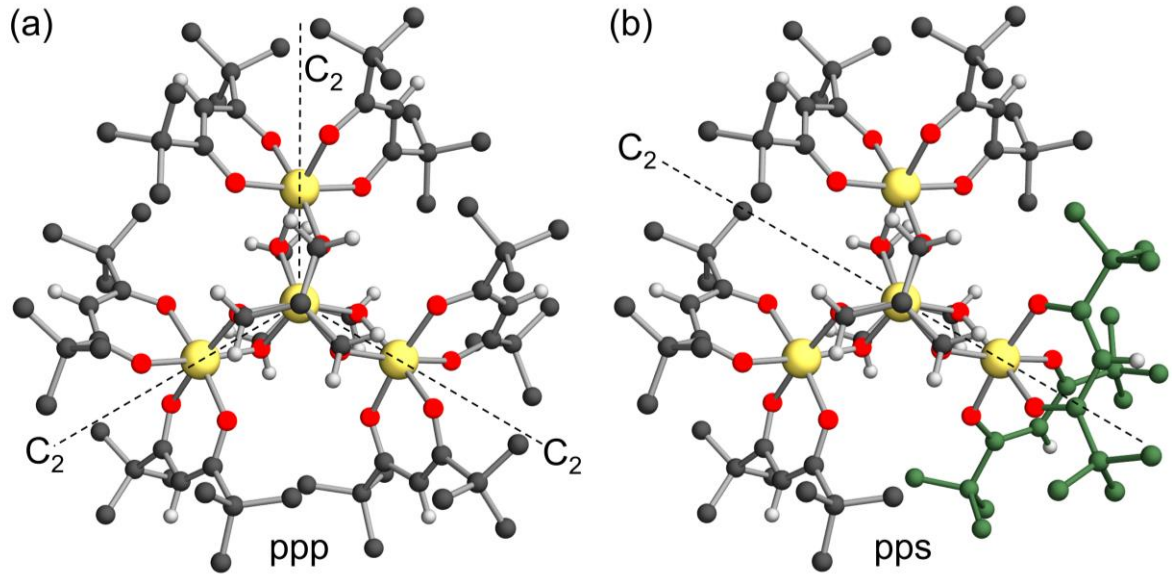

Figure 2. Molecular structure of ppp (a) and pps (b) isomers in $\mathbf{1^{4\text{-}Py}}$·EtOH, viewed normal to the molecular plane. For clarity, the 4-pyridyl groups and the minority components of disordered *t*Bu substituents, as well as *t*Bu hydrogens, are omitted. The dashed lines are the twofold axes required by idealized D_3 (a) and C_2 (b) symmetry. The same color code as in Figure 1 is used for Ga, O, C and H atoms, but the carbon atoms of the two dpm^- ligands in *sandwich*-like coordination mode (b) are drawn in green.

NMR spectra. NMR spectroscopy was extensively used to investigate diamagnetic polynuclear species, among which Werner's hexols[22] and Group 13 complexes.[11,12,14] A freshly prepared solution of $\mathbf{1^{4\text{-}Py}}$·EtOH in C_6D_6 affords a very rich and well-resolved ^{1}H NMR spectrum (Figures 3 and S2-S8). We first focus on the aromatic region, which contains characteristic multiplets of the 4-pyridyl substituents on the tripodal ligands (Figure 3a). By comparison with the spectrum of the $H_3L^{4\text{-}Py}$ proligand alone,[52] the signal at 8.54 ppm is attributed to the *alpha* protons and is mirrored by a minor peak with similar structure at 8.49 ppm, whose integrated intensity amounts to ca. 1/3 of that of the main peak (the total area of these two signals was calibrated to 4H). A similar pattern is visible in the chemical shift region of *beta* protons, with a main peak at 7.44 ppm and a minor peak at 7.33 ppm (~3:1 ratio, 4H overall). Other barely visible peaks of similar shape are present in the aromatic region (8.43 and 7.21 ppm), with integrated intensity that however does not exceed a few percent of the dominant signals (see also Figure S8c). Thus, two inequivalent 4-pyridyl groups are present in solution in a ~3:1 ratio, along with traces of a third distinct 4-pyridyl residue (neglected in the following).

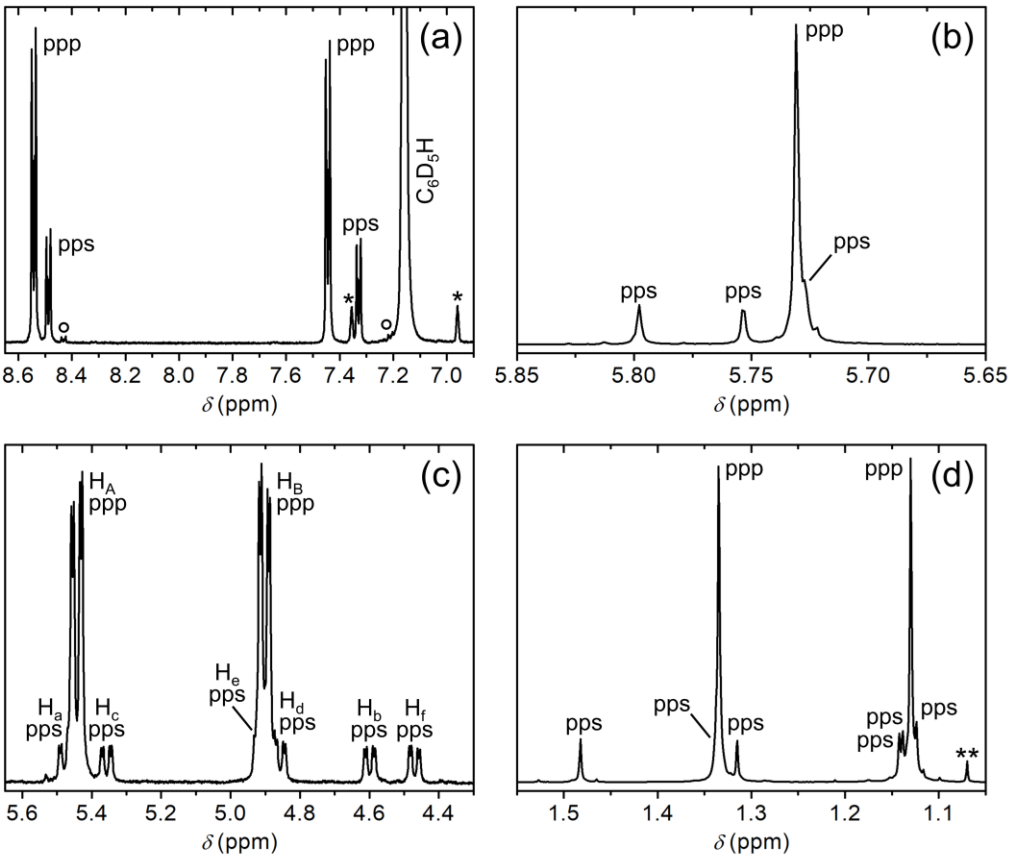

Figure 3. ^{1}H NMR spectrum of **1$^{4\text{-Py}}$**·EtOH (400.13 MHz, C_6D_6, 298 K), with the assignment of the peaks to ppp and pps isomers. ***** = satellite peaks of solvent signal at 7.16 ppm, ○ = *α*-H and *β*-H peaks of pss isomer (tentative), ** traces of free Hdpm (*t*Bu).

The spectral region from 5.8 to 5.7 ppm (Figure 3b) contains the resonances of dpm^- methine hydrogens, as suggested by the ^{1}H NMR spectrum of $Ga(dpm)_3$ in C_6D_6 [53] and confirmed by the total integrated intensity (6H). The observed signals are a dominant singlet at 5.73 ppm (~5H) *plus* two weaker signals at 5.80 (~0.5H) and 5.75 ppm (~0.5H). In addition, a shoulder is visible on the high-field side of the main peak, suggesting the presence of *four* distinct methine hydrogens in a 4.5:0.5:0.5:0.5 ratio.

Several doublets-of-doublets (dd) appear between 5.6 and 4.4 ppm (Figure 3c), with overall integrated area amounting to 12H and thus attributable to CH_2 hydrogens of the tripodal ligands. These methylene groups are observed around 4 ppm in the free proligand[52] and, as found in an isostructural derivative,[36] undergo a downfield shift upon complexation. It appears that two main signals at 5.44 (H_A) and 4.90 ppm (H_B), amounting to ~4.5H each, are accompanied by six weaker dd peaks: H_a at 5.48 (partially overlapping with the main component), H_c at 5.36, H_e at 4.92 (overlapping with the main component), H_d at 4.86, H_b at 4.60 and H_f at 4.47 ppm, each one

amounting to ~0.5H (overlapping signals are clearly resolved in ^{1}H,^{1}H-COSY experiments, see Figures S8a and S8b). In all these signals, the larger splitting is 9.7-9.8 Hz while the smaller splitting amounts to 2.7-2.8 Hz.

In the *t*Bu region from 1.5 to 1.1 ppm[53] (Figure 3d) two dominant singlets are found at 1.33 and 1.13 ppm, while weaker peaks of approximately equal intensity occur at 1.48, 1.32, 1.14 (×2) and 1.12 ppm. Moreover, a shoulder is visible on the low-field side of the 1.33-ppm peak. The four lowest-field and the four highest-field peaks in this spectral region both sum to ~54H, suggesting that the 12 *t*Bu groups of dpm^{-} ligands can be grouped into two main types.

In sharp contrast with Figure 3, the ^{1}H NMR spectra of [$Fe^{III}_{3}M^{III}(L^{R})_{2}(dpm)_{6}$] complexes are dominated by the very broad, paramagnetically-shifted band of *t*Bu protons, while methine protons appear as a barely visible band at negative δ values and CH_2 hydrogens of tripodal ligands are undetectable.[30,36,39,40]

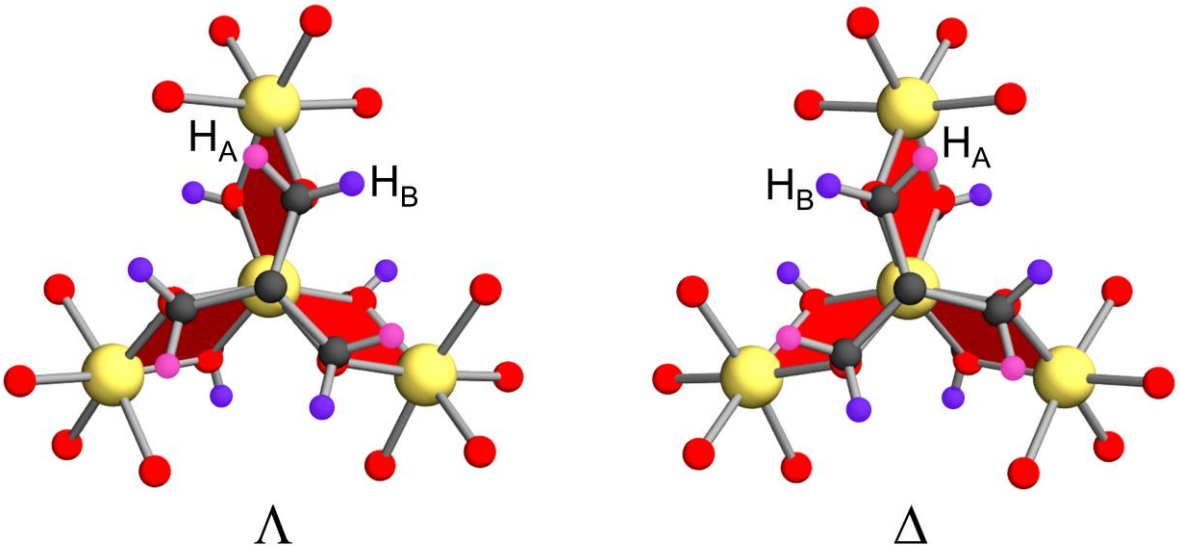

Figure 4. Structure of the Λ and Δ enantiomers of **1$^{4\text{-Py}}$** (ppp isomer) omitting C and H atoms of dpm^{-} ligands and the 4-pyridyl groups. The color code for Ga, O and C atoms is the same as in Figure 1, but the color of H atoms indicates equivalence in D_3 symmetry within each enantiomer. The diastereotopic CH_2 hydrogens are assigned as H_A and H_B based on DFT calculations. Configuration inversion transforms the pink (purple) H_A (H_B) atoms of Λ isomer into H_B (H_A) atoms of Δ isomer.

All the dominant peaks in the spectrum are consistent (in number and integrated intensity) with a D_3-symmetric structure over the NMR timescale. Since the pyridyl ring is expected to rotate freely in solution, this is the symmetry expected for the ppp isomer (Figure S9). Its six dpm^{-} ligands would in fact be equivalent, affording *one* methine singlet and *two* signals of equal intensity from the two

symmetry-inequivalent *t*Bu groups within each dpm^- ligand. Tripodal ligands would contain six equivalent CH_2 groups; however, the *two* signals of equal intensity detected at 5.44 and 4.90 ppm (Figure 3c) indicate that the two protons in each CH_2 group (H_A and H_B) are *diastereotopic*, as previously suggested for an isostructural derivative[36] and for Group 13 alkoxides with a propeller-like structure.[10,12,13,17,45–47] Since interconversion between Λ and Δ propeller's isomers (racemization)[54] exchanges the position of these protons (Figure 4), it follows that the process must be slower than NMR timescale.

As mentioned above, the two signals appear as doublets-of-doublets, the larger splitting (9.7-9.8 Hz) falling in the range expected for geminal coupling ($^2J_{H,H}$). The additional splitting by 2.7-2.8 Hz is presumably long-range in origin and related to the particular structure of the tripodal ligand. In fact, the six CH_2O protons of each tripodal ligand form an AA'A"BB'B" system that gives a deceptively simple spectrum in which the 5.44-ppm proton of one methylene group is long-range coupled ($^4J_{H,H}$) to the 4.90-ppm proton of another methylene group.

These findings are correctly reproduced and rationalized by density functional theory (DFT) calculations, based on crystallographic coordinates (except for hydrogen atoms, which were optimized). To this aim, two models (M1 and M2) were employed (see Experimental Section). M1 is the whole neutral ppp isomer of **1$^{4\text{-Py}}$** and was used to compute the chemical shifts (δ_{calc}) of the protons belonging to the tripodal ligands (see Figure S10 and Table S1). The aromatic protons are predicted to resonate at average chemical shift values of 8.61 ppm (*alpha* protons) and 7.61 ppm (*beta* protons), in good agreement with experiment (8.49 and 7.44 ppm, respectively). The signals of methylene groups of tripodal ligands can be found between 4 and 6 ppm, and the two geminal protons inside the same CH_2 group are clearly diastereotopic, with average δ_{calc} values of 5.60 and 4.93 ppm. These calculated chemical shifts compare well with the experimental values of 5.44 (H_A) and 4.90 ppm (H_B). Calculations then prove that H_A is the CH_2 proton lying closer to the neighboring Ga_p atom, as shown in Figure 4.

M2 consists in the $[Ga(L^{4\text{-Py}})_2]^{3-}$ fragment, i.e. the two tripodal $(L^{4\text{-Py}})^{3-}$ ligands and the central Ga^{3+} ion (Figure S10). This truncated model was used to compute the scalar coupling constants among the methylene protons of the two tripodal ligands (see Table S2), as calculations on the complete structure (M1) would be too demanding. The results clearly show that two types of interaction pathways dominate: i) the geminal coupling, with an average $^2J_{H,H}$ value of –8.2 Hz; ii) the interaction between two diastereotopic protons of two different CH_2 groups belonging to the same tripodal ligand ($^4J_{H,H}$ = 3.4 Hz on average). The pairs of long-range interacting hydrogens are the ones exhibiting a "W" arrangement (Figure S10 and Table S2), a phenomenon known as "propanic coupling" and occurring over four saturated bonds.[55] Other long-range interactions involving CH_2 hydrogens, like

those with the aromatic protons and those between CH_2 groups of different tripodal ligands, are very weak (<1 Hz). The calculated *J* values are in satisfactory agreement with the experimental data, even if geminal coupling is underestimated by ca. 15% and long-range coupling is overestimated by ca. 25%. These deviations might reflect differences between solid-state and solution structures. Interestingly, truncated model M2 results in no clear chemical shift differentiation between the two structurally inequivalent CH_2 protons (see Table S3), indicating that the distinct δ_{calc} values of H_A and H_B are a consequence of the overall molecular structure.

Significantly, all peaks of the majority species (except for those of aromatic protons) are *tripled* in the minority species. It follows that one-fourth of the molecules in solution have a symmetry lower than D_3 over NMR timescale. We contend that such symmetry lowering arises from the occurrence of a *sandwich*-like (s) arrangement of dpm^- ligands around *one* gallium(III) ion, i.e. from the stereoisomerism revealed by the X-ray diffraction analysis. Indeed, assuming free rotation of the 4-pyridyl group, the C_2–symmetric pps isomer leads to *three* types of methine, *six* types of CH_2 and *six* types of *t*Bu hydrogens, exactly as observed (Figure S11). The six methylene signals exhibit a virtually identical shape to peaks H_A and H_B of ppp isomer. As shown by DFT calculations, this shape is indicative of two *diastereotopic*, geminally coupled protons per CH_2 group and of additional long-range interactions within the tripodal ligand. This result is consistent with the proposed assignment, as the symmetry lowering from D_3 to C_2 largely preserves the conformation of the tripodal ligand and is expected to have a much larger impact on proton chemical shifts than on *J* values. The coupling network of methylene hydrogens within pps isomer can be inferred from the intensity of the cross-peaks in the $^1H,^1H$-COSY spectrum (higher for geminal couplings and lower for long-range couplings). From Figures S8a and S8b it is clear that geminal couplings involve H_a-H_b, H_c-H_d, and H_e-H_f, whereas long-range couplings involve H_a-H_e, H_b-H_c, and H_d-H_f.

In support of the proposed interpretation, the calculated relative amount of ppp and pps+psp isomers in the solid (2.61) is close to the ppp/pps ratio detected in freshly-prepared C_6D_6 solutions (~3). It must be noted, however, that this ratio was found to slowly increase upon standing and reached ~5:1 after 2 h. The possibility to observe separate NMR signals for the two isomeric forms of $\mathbf{1^{4\text{-}Py}}$ indicates that interconversion of ppp and pps isomers, like racemization and exchange of dpm^- ligands,[35] is a slow process over NMR timescale. An attempt was made to observe linewidth changes due to exchange processes in C_6D_6 in the temperature range between 5 and 45 °C, but no variations were appreciated. Traces of the pss complex are presumably responsible for the very weak 4-pyridyl signals detected at 8.43 and 7.21 ppm. Interestingly, this assignment implies that aromatic protons undergo a progressive upfield shift with increasing number of s-mode ligands.

The ^{1}H NMR spectrum of a freshly-prepared solution of **1$^{4\text{-Py}}$**·EtOH in CD_2Cl_2 shows a similar pattern of signals consistent with the presence of D_3- and C_2-symmetric species, again in a ~3:1 molar ratio (Figure S2).

We finally notice that **1^{Ph}**·Et_2O, dissolved in C_6D_6, gives a similar ^{1}H NMR spectral pattern, though with a distinctly higher ppp/pps ratio (ca. 7, evaluated from *ortho* phenyl protons).[36] Re-consideration of single-crystal X-ray diffraction data from our archives indeed showed hints of disorder in the coordination sphere of Ga3. When such disorder was disregarded, as done in Ref.[36], the largest electron density residual was only 0.9 eÅ^{-3} vs. 1.4 eÅ^{-3} in **1$^{4\text{-Py}}$**·EtOH, confirming that this type of stereoisomerism occurs to a smaller extent in **1^{Ph}**·Et_2O than in **1$^{4\text{-Py}}$**·EtOH.

CONCLUSION

The structure of propeller-like SMMs with formula $[Fe^{III}_3M^{III}(L^R)_2(dpm)_6]$ is difficult to investigate in solution by ^{1}H NMR spectroscopy due to the paramagnetic broadening of resonance lines. A tetragallium(III) complex, $[Ga_4(L^{4\text{-Py}})_2(dpm)_6]$ (**1$^{4\text{-Py}}$**), was synthesized in racemic form and structurally and spectroscopically characterized as an isostructural diamagnetic analogue. Compound **1$^{4\text{-Py}}$**·EtOH gives spectacular ^{1}H NMR spectra in C_6D_6, showing that the molecule achieves D_3 symmetry in solution and that Λ and Δ propeller's isomers are configurationally stable over NMR timescale. Key information was provided by the NMR resonances of the tripodal $(L^{4\text{-Py}})^{3-}$ ligands, whose CH_2 hydrogens become diastereotopic, in agreement with DFT calculations. As previously found in Fe^{3+}-based propeller-like complexes,[41,42,49–51] the partly disordered coordination sphere of Ga_p ions in crystalline **1$^{4\text{-Py}}$**·EtOH suggests the occurrence of stereoisomers with lower symmetry. Such additional stereoisomerism shows up clearly in the ^{1}H NMR spectra of **1$^{4\text{-Py}}$**·EtOH as a set of weaker resonances that are consistent with a C_2-symmetric molecule.

Considering the distinctly more labile character of Ga^{3+} vs Fe^{3+} complexes,[32,33] the above-presented conclusions on configurational stability are expected to hold for the vast pool of Fe^{III}_4, $Fe^{III}_3Cr^{III}$ and $Fe^{III}_3V^{III}$ SMMs containing $(L^R)^{3-}$ tripods and peripheral dpm^- ligands.[25]

EXPERIMENTAL SECTION

General methods. Piperidine (Carlo Erba, 99%), $GaCl_3$ (Sigma Aldrich, 99.99%), CH_2Cl_2 (Sigma Aldrich, anhydrous, 99.8%) and ^{i}PrOH (Supelco, ≥99.9%) were used as received. Diethyl ether (Sigma Aldrich, reagent grade, pre-dried over $CaCl_2$ for 24 h) and ethanol (Fluka, reagent grade) were

distilled from sodium diphenylketyl solution and from magnesium ethoxide, respectively, prior to use.[56] The tripodal ligand $H_3L^{4\text{-Py}}$ was prepared by reacting 4-picoline with formaldehyde, as previously described.[38,52] $[Ga_2(OMe)_2(dpm)_4]$ (**4**) was obtained as reported elsewhere.[36]

Elemental analyses were performed using a Carlo Erba EA1110 CHNS-O automatic analyzer. Infrared spectra were recorded as KBr disks using a Jasco FTIR-4700LE spectrophotometer with a 2 cm^{-1} resolution.

^1H NMR spectra in C_6D_6 (8.0 mg in 0.6 mL) and CD_2Cl_2 (6.0 mg in 0.6 mL) were recorded at room temperature on Bruker AVANCE400 and DPX200 FT-NMR spectrometers at 400.13 MHz and 200.13 MHz, respectively; additional measurements were made in C_6D_6 at 400.13 MHz between 5 and 45 °C; chemical shifts δ are given versus external tetramethylsilane (TMS). The spectra were calibrated setting the solvent residual proton signals at 7.16 and 5.32 ppm, respectively, in the two solvents.[57] The following abbreviations are used in reporting NMR data: s = singlet, t = triplet, q = quartet, dd = doublet-of-doublets, m = multiplet. Geminal coupling constants ($^2J_{H,H}$) are quoted with a negative sign, as appropriate for methylene groups,[58] although in our case the sign cannot be directly determined from the ^1H NMR spectrum.

ESI-MS measurements were conducted on a 6310A Ion Trap LC-MS(n) instrument (Agilent Technologies), by direct infusion of an ^{i}PrOH : CH_2Cl_2 (3:1 v/v) solution and working in positive ion mode.

$[Ga_4(L^{4\text{-Py}})_2(dpm)_6]\cdot$EtOH ($1^{4\text{-Py}}\cdot$EtOH). A solution of $GaCl_3$ (12.5 mg, 0.0710 mmol) in EtOH (2.5 mL) was treated with solid **4** (100 mg, 0.107 mmol) and then with Et_2O (10 mL). The mixture was stirred until virtually complete dissolution. Addition of piperidine (29 μL, 25 mg, 0.29 mmol) caused precipitation of a white microcrystalline solid (piperidinium chloride). The mixture was treated with $H_3L^{4\text{-Py}}$ (52 mg, 0.28 mmol) suspended in EtOH (1.5 mL), and stirred for 3 h, after which time the precipitate was filtered off over a G4 glass frit. Slow vapor diffusion of EtOH (25 mL) into the filtrate gave off-white rod-like crystals of $\mathbf{1}^{4\text{-Py}}\cdot$EtOH, that were collected by filtration, washed with the diffusion solvent mixture and rapidly dried under vacuum (91 mg, 72%). ^1H NMR (400.13 MHz, C_6D_6, 298 K): for ppp isomer (molar fraction ~ 0.75) δ = 8.54 (m AA′, 4H; α-H), 7.44 (m BB′, 4H; β-H), 5.73 (s, 6H; =CH), 5.44 (dd, 6H, $^2J_{H,H}$ = –9.7 Hz, $^4J_{H,H}$ = 2.8 Hz; H_ACH_B), 4.90 (dd, 6H, $^2J_{H,H}$ = –9.7 Hz, $^4J_{H,H}$ = 2.8 Hz; H_ACH_B), 1.33 (s, 54H; *t*Bu), 1.13 ppm (s, 54H; *t*Bu); for pps isomer (molar fraction ~ 0.25) δ = 8.49 (m AA′, 4H; α-H), 7.33 (m BB′, 4H; β-H), 5.80 (s, 2H; =CH), 5.75 (s, 2H; =CH), 5.73 (s, 2H; =CH), 5.48 (dd, 2H, $^2J_{H,H}$ = –9.7 Hz, $^4J_{H,H}$ = 2.7 Hz; H_aCH_b), 5.36 (dd, 2H, $^2J_{H,H}$ = –9.8 Hz, $^4J_{H,H}$ = 2.8 Hz; H_cCH_d), 4.92 (dd, 2H, $^2J_{H,H}$ = –9.7 Hz, $^4J_{H,H}$ = 2.7 Hz; H_eCH_f), 4.86 (dd, 2H, $^2J_{H,H}$ = –9.8 Hz, $^4J_{H,H}$ = 2.7 Hz; H_cCH_d), 4.60 (dd, 2H, $^2J_{H,H}$ = –9.7 Hz, $^4J_{H,H}$ = 2.8 Hz; H_aCH_b),

4.47 (dd, 2H, $^{2}J_{H,H}$ = –9.7 Hz, $^{4}J_{H,H}$ = 2.7 Hz; H_eCH_f), 1.48 (s, 18H; *t*Bu), 1.34 (s, 18H; *t*Bu), 1.32 (s, 18H; *t*Bu), 1.14_2 (s, 18H; *t*Bu,), 1.13_8 (s, 18H; *t*Bu,), 1.12 ppm (s, 18H; *t*Bu); ethanol (0.95 mol per mole of **1$^{4\text{-Py}}$**) δ = 3.31 (q, 2H, $^{3}J_{H,H}$ = 7.0 Hz; CH_2), 0.94 (t, 3H, $^{3}J_{H,H}$ = 7.0 Hz; CH_3), 0.52 ppm (s, br; OH+H_2O); diethyl ether (0.13 mol per mole of **1$^{4\text{-Py}}$**) δ = 3.26 (q, 4H, $^{3}J_{H,H}$ = 7.0 Hz; CH_2), 1.11 ppm (t, 6H, $^{3}J_{H,H}$ = 7.0 Hz; CH_3); IR (KBr): $\tilde{\nu}$ = 3388 (br), 2964 (s), 2927 (s), 2907 (s), 2868 (s), 1598 (vs), 1571 (vs), 1554 (vs), 1540 (vs), 1508 (vs), 1451 (s), 1416 (vs), 1382 (s), 1359 (vs), 1296 (w), 1250 (m), 1227 (m), 1183 (m), 1147 (m), 1103 (s), 1075 (m), 963 (m), 951 (m), 875 (s), 813 (w), 793 (s), 765 (w), 744 (w), 666 (m), 630 (m), 597 (s), 565 (m), 485 (m), 443 (m) cm^{-1}; ESI-MS: *m*/*z* (%) = 1761.7 (100) [**1$^{4\text{-Py}}$**+Na]$^+$, 1745.8 (8) [**1$^{4\text{-Py}}$**+Li]$^+$, 1739.6 (2) [**1$^{4\text{-Py}}$**+H]$^+$; elemental analysis calcd (%) for $C_{86}H_{140}Ga_4N_2O_{19}$ (1784.93): C 57.87, H 7.91, N 1.57; found: C 58.20, H 8.17, N 1.80.

X-ray Crystallography. Single-crystal X-ray structure determination on **1$^{4\text{-Py}}$**·EtOH was carried out at 140(2) K on a Bruker-Nonius X8APEX diffractometer equipped with Mo-Kα generator, area detector and Kryoflex liquid dinitrogen cryostat. Structure solution and refinement on F_o^2 were carried out by standard methods, utilizing SIR92[59] and SHELXL-2018/3[60] software and the WINGX v2020.2 suite.[61] All nonhydrogen atoms were refined anisotropically, unless otherwise noted. A riding model was used for hydrogen atoms, which were added in idealized positions and treated isotropically with U(H) = 1.5U_{eq}(X) for methyl and hydroxyl hydrogens, and U(H) = 1.2U_{eq}(C) for the remaining hydrogen atoms.

The coordination environment of the gallium(III) ions lying on the twofold axis (Ga1 and Ga2) is ordered within experimental resolution, except for a rotationally disorder *t*Bu group in the two symmetry-related dpm^- ligands (dpm1) bound to Ga2 [0.614(7):0.386(7)]. By contrast, the two dpm^- ligands coordinated to Ga3 (dpm2 and dpm3) exhibit both *propeller*-like (p) and *sandwich*-like (s) coordination modes, with 0.8393(18) and 0.1607(18) occupancies, respectively, but unresolved splitting of O atoms. Upon neglection of the disorder, R_1 increases from 4.21 to 5.95% and the carbon atoms of s-mode β-diketonato moieties show up clearly as electron density residuals of up to 1.4 eÅ^{-3}. A *t*Bu group of dpm2 in its prevalent p-mode arrangement is detectably disordered over two positions [0.453(3):0.386(3)], which were refined by restraining (DFIX) the C(O)-C(CH_3)$_3$ bond distances to 1.540(5) Å. All disordered *t*Bu groups were treated with restraints based on the geometry of the ordered *tert*-butyl of dpm1 (SAME), with enhanced rigid-body restraints (RIGU) on anisotropic displacement parameter (ADPs)[62] and an identity ADP constraint (EADP) on split quaternary carbons. The minority s-mode components were restrained to be geometrically similar to dpm1 (SAME) and only two isotropic displacement parameters were used, one for *t*Bu methyl carbons and one for the remaining C atoms.

A half-occupancy EtOH molecule with large displacement parameters was located in the asymmetric unit at hydrogen-bond distance from the 4-pyridyl nitrogen, as confirmed by the broad band at 3388 cm^{-1} in the FT-IR spectra. This results in one EtOH per tetragallium(III) complex and is consistent with NMR analysis. It was refined over two positions [0.394(8):0.106(8)] with coinciding carbons but distinct O atoms. C-O and C-C distances were restrained (DFIX) to 1.430(15) and 1.510(15) Å, respectively. The minority O atom was treated isotropically, while the remaining atoms were forced to approximate isotropic behaviour (ISOR). Hydroxyl hydrogens were refined using a riding model (AFIX 83). Graphics utilized ORTEP-3 for Windows v2014.1[61] and POV-Ray for Windows v3.7.[63] *Crystal data*: $C_{86}H_{140}Ga_4N_2O_{19}$, M = 1784.87 g mol^{-1}, crystal size 0.54×0.18×0.12 mm^3, monoclinic, space group $C2/c$, a = 19.3203(9), b = 21.9357(11), c = 23.7468(12) Å, β = 106.612(2)°, V = 9644.0(8) $Å^3$, Z = 4, ρ_{calc} = 1.229 g cm^{-3}, θ_{max} = 28.03°, T = 140(2) K, collected/independent reflections = 49874/11637, parameters/restraints = 652/351, R(int) = 0.0353, final indices R_1 = 0.0421, wR_2 = 0.1153 [on reflections with $I > 2\sigma(I)$], R_1 =0.0737, wR_2 = 0.1274 [on all data], GOF = 1.063.

Deposition Number CCDC 2114257 (for **$1^{4\text{-Py}}$**·EtOH) contains the supplementary crystallographic data for this paper. These data are provided free of charge by the joint Cambridge Crystallographic Data Centre and Fachinformationszentrum Karlsruhe Access Structures service.

Density Functional Theory (DFT) Calculations. All DFT calculations were performed with ORCA 4.2.1 quantum chemistry package.[64] Two different molecular models were employed. Model 1 (M1) is the whole neutral ppp isomer of **$1^{4\text{-Py}}$**. Model 2 (M2) is a trianion constituted by the two tripodal ligands $(L^{4\text{-Py}})^{3-}$ and the central Ga^{3+} ion (Figure S10). In both models the crystallographic coordinates of the ppp isomer were employed for all the atoms except H (disordered moieties were set in their largest occupancy positions). Hydrogen atom positions were optimized in presence of an implicit solvent model, Conductor-like Polarizable Continuum Model (CPCM), to mimic the benzene solvent.[65] For the geometry optimizations, PBE functional[66] and D3 empirical dispersion correction[67,68] were used, while def2-SVP basis set[69] was employed for all the atoms. TMS molecule was optimized at the same level of theory to serve as a reference for ^{1}H chemical shifts.

To compute the NMR parameters, single point calculations with hybrid B3LYP functional[70,71] were performed on the final optimized geometries. Chemical shift values were obtained on both complete model M1 (δ_{M1}) and truncated model M2 (δ_{M2}). Due to the limited computational resources, calculations on M1 utilized PCSSEG-2 basis set[72] only for the hydrogen atoms of $(L^{4\text{-Py}})^{3-}$ ligands, and def2-SVP basis for all other atoms. The PCSSEG-2 basis set was used for all atoms of M2. The chemical shift of TMS protons (δ_{TMS}) was simulated at the same level of theory to serve as a reference, and the final chemical shifts were computed as $\delta_{calc} = \delta_{TMS} - \delta_{M1/2}$ for comparison with experimental

data. Since $\mathbf{1^{4\text{-}Py}}$ is made of 242 atoms and the calculation of NMR parameters is computationally demanding, the scalar coupling constants (*J*) among protons of the tripodal ligands were computed on truncated model M2 only.

ACKNOWLEDGEMENTS

This work was supported by Italian MIUR through a FIRB project (RBAP117RWN). The authors thank Dr. Luca Rigamonti for preliminary studies and assistance in the preparation of bulk samples.

Keywords: density functional calculations; gallium; NMR spectroscopy; single-molecule magnet; tripodal ligands

References

[1] I. Bernal, J. Cetrullo, S. Berhane, *J. Coord. Chem.* **2000**, *52*, 185–205.

[2] G. B. Kauffman, *Coord. Chem. Rev.* **1973**, *9*, 339–363.

[3] U. Thewalt, *Chem. Ber.* **1971**, *104*, 2657–2669.

[4] A. Konishi, H. Nakajima, H. Maruyama, S. Yoshioka, A. Baba, M. Yasuda, *Polyhedron* **2017**, *125*, 130–134.

[5] M. Hu, F. Wang, F. Han, Q. Deng, W. Ma, H. Yan, G. Dong, W. Song, *J. Polym. Sci., Part A: Polym. Chem.* **2017**, *55*, 2084–2091.

[6] A. A. Ali, V. Huch, C. Aktas, M. Veith, *Z. Anorg. Allg. Chem.* **2016**, *642*, 973–978.

[7] X. Li, V. K. Michaelis, T.-C. Ong, S. J. Smith, I. McKay, P. Müller, R. G. Griffin, E. N. Wang, *CrystEngComm* **2014**, *16*, 2950–2958.

[8] S. Mishra, V. Mendez, E. Jeanneau, V. Caps, S. Daniele, *Eur. J. Inorg. Chem.* **2013**, 500–510.

[9] E. J. Bierschenk, N. R. Wilk, T. P. Hanusa, *Inorg. Chem.* **2011**, *50*, 12126–12132.

[10] A. Mitra, Y. Wang, S. Parkin, D. Atwood, *Dalton Trans.* **2008**, 1037–1042.

[11] C. J. Carmalt, S. J. King, *Coord. Chem. Rev.* **2006**, *250*, 682–709.

[12] B. Neumüller, *Chem. Soc. Rev.* **2003**, *32*, 50–55.

[13] S. Chitsaz, B. Neumüller, *Z. Anorg. Allg. Chem.* **2001**, *627*, 2451–2459.

[14] M.-A. Munoz-Hernandez, P. Wei, S. Liu, D. A. Atwood, *Coord. Chem. Rev.* **2000**, *210*, 1–10.

[15] S. Suh, D. M. Hoffman, *J. Am. Chem. Soc.* **2000**, *122*, 9396–9404.

[16] A. Duda, S. Penczek, *Macromol. Rapid Commun.* **1995**, *16*, 67–76.

[17] R. Kumar, V. S. J. de Mel, M. L. Sierra, D. G. Hendershot, J. P. Oliver, *Organometallics* **1994**, *13*, 2079–2083.

[18] L. J. Batchelor, M. Sander, F. Tuna, M. Helliwell, F. Moro, J. van Slageren, E. Burzurí, O. Montero, M. Evangelisti, F. Luis, E. J. L. McInnes, *Dalton Trans.* **2011**, *40*, 5278–5284.

[19] P. Andersen, T. Damhus, E. Pedersen, A. Petersen, *Acta Chem. Scand., Ser. A* **1984**, *38*, 359–376.

[20] H. U. Güdel, U. Hauser, *Inorg. Chem.* **1980**, *19*, 1325–1328.

[21] J. Mayans, M. Font-Bardia, A. Escuer, *Dalton Trans.* **2018**, *47*, 8392–8401.

[22] D. A. Marsh, W. S. Elliott, R. M. Smith, M. C. Sharps, M. K. Baumeister, M. E. Carnes, L. N. Zakharov, W. H. Casey, D. W. Johnson, *Angew. Chem. Int. Ed.* **2017**, *56*, 8776–8779; *Angew. Chem.* **2017**, *129*, 8902–8905.

[23] D. J. Hodgson, K. Michelsen, E. Pedersen, D. K. Towle, *Inorg. Chem.* **1991**, *30*, 815–822.

[24] S. Müller, U. Thewalt, *Z. Naturforsch., B: J. Chem. Sci.* **1989**, *44*, 257–260.

[25] A. Cornia, M. Mannini, R. Sessoli, D. Gatteschi, *Eur. J. Inorg. Chem.* **2019**, 552–568.

[26] P. Totaro, K. C. M. Westrup, M.-E. Boulon, G. G. Nunes, D. F. Back, A. Barison, S. Ciattini, M. Mannini, L. Sorace, J. F. Soares, A. Cornia, R. Sessoli, *Dalton Trans.* **2013**, *42*, 4416–4426.

[27] L. Sorace, M.-E. Boulon, P. Totaro, A. Cornia, J. Fernandes-Soares, R. Sessoli, *Phys. Rev. B: Condens. Matter Mater. Phys.* **2013**, *88*, 104407.

[28] M. Mannini, E. Tancini, L. Sorace, P. Sainctavit, M.-A. Arrio, Y. Qian, E. Otero, D. Chiappe, L. Margheriti, J. C. Cezar, R. Sessoli, A. Cornia, *Inorg. Chem.* **2011**, *50*, 2911–2917.

[29] E. Tancini, M. Mannini, P. Sainctavit, E. Otero, R. Sessoli, A. Cornia, *Chem. - Eur. J.* **2013**, *19*, 16902–16905.

[30] K. C. M. Westrup, M.-E. Boulon, P. Totaro, G. G. Nunes, D. F. Back, A. Barison, M. Jackson, C. Paulsen, D. Gatteschi, L. Sorace, A. Cornia, J. F. Soares, R. Sessoli, *Chem. - Eur. J.* **2014**, *20*, 13681–13691.

[31] R. D. Shannon, C. T. Prewitt, *Acta Crystallogr., Sect. B: Struct. Crystallogr. Cryst. Chem.* **1970**, *26*, 1046–1048.

[32] D. Hugi-Cleary, L. Helm, A. E. Merbach, *J. Am. Chem. Soc.* **1987**, *109*, 4444–4450.

[33] J. L. Brumaghim, K. N. Raymond, *J. Am. Chem. Soc.* **2003**, *125*, 12066–12067.

[34] A. Repollés, A. Cornia, F. Luis, *Phys. Rev. B: Condens. Matter Mater. Phys.* **2014**, *89*, 054429.

[35] L. Vergnani, A.-L. Barra, P. Neugebauer, M. J. Rodriguez-Douton, R. Sessoli, L. Sorace, W.

Wernsdorfer, A. Cornia, *Chem. - Eur. J.* **2012**, *18*, 3390–3398.

[36] E. Tancini, M. J. Rodriguez-Douton, L. Sorace, A.-L. Barra, R. Sessoli, A. Cornia, *Chem. - Eur. J.* **2010**, *16*, 10482–10493.

[37] L. Rigamonti, C. Cotton, A. Nava, H. Lang, T. Rüffer, M. Perfetti, L. Sorace, A.-L. Barra, Y. Lan, W. Wernsdorfer, R. Sessoli, A. Cornia, *Chem. - Eur. J.* **2016**, *22*, 13705–13714.

[38] A. Nava, L. Rigamonti, E. Zangrando, R. Sessoli, W. Wernsdorfer, A. Cornia, *Angew. Chem. Int. Ed.* **2015**, *54*, 8777–8782; *Angew. Chem.* **2015**, *127*, 8901–8906.

[39] L. Rigamonti, M. Piccioli, L. Malavolti, L. Poggini, M. Mannini, F. Totti, B. Cortigiani, A. Magnani, R. Sessoli, A. Cornia, *Inorg. Chem.* **2013**, *52*, 5897–5905.

[40] G. G. Condorelli, A. Motta, G. Pellegrino, A. Cornia, L. Gorini, I. L. Fragalà, C. Sangregorio, L. Sorace, *Chem. Mater.* **2008**, *20*, 2405–2411.

[41] A. L. Barra, A. Caneschi, A. Cornia, F. Fabrizi de Biani, D. Gatteschi, C. Sangregorio, R. Sessoli, L. Sorace, *J. Am. Chem. Soc.* **1999**, *121*, 5302–5310.

[42] S. Accorsi, A.-L. Barra, A. Caneschi, G. Chastanet, A. Cornia, A. C. Fabretti, D. Gatteschi, C. Mortalò, E. Olivieri, F. Parenti, P. Rosa, R. Sessoli, L. Sorace, W. Wernsdorfer, L. Zobbi, *J. Am. Chem. Soc.* **2006**, *128*, 4742–4755.

[43] K. L. Mears, L. G. Bloor, D. Pugh, A. E. Aliev, C. E. Knapp, C. J. Carmalt, *Inorg. Chem.* **2019**, *58*, 10346–10356.

[44] S. Mishra, S. Daniele, S. Petit, E. Jeanneau, M. Rolland, *Dalton Trans.* **2009**, 2569–2577.

[45] S. Basharat, W. Betchley, C. J. Carmalt, S. Barnett, D. A. Tocher, H. O. Davies, *Organometallics* **2007**, *26*, 403–407.

[46] S. Chitsaz, E. Iravani, B. Neumüller, *Z. Anorg. Allg. Chem.* **2002**, *628*, 2279–2285.

[47] M. Valet, D. M. Hoffman, *Chem. Mater.* **2001**, *13*, 2135–2143.

[48] L. Gregoli, C. Danieli, A.-L. Barra, P. Neugebauer, G. Pellegrino, G. Poneti, R. Sessoli, A. Cornia, *Chem. - Eur. J.* **2009**, *15*, 6456–6467.

[49] A. Bouwen, A. Caneschi, D. Gatteschi, E. Goovaerts, D. Schoemaker, L. Sorace, M. Stefan, *J. Phys. Chem. B* **2001**, *105*, 2658–2663.

[50] L. Rigamonti, A. Nava, M.-E. Boulon, J. Luzon, R. Sessoli, A. Cornia, *Chem. - Eur. J.* **2015**, *21*, 12171–12180.

[51] L. Rigamonti, A. Cornia, A. Nava, M. Perfetti, M.-E. Boulon, A.-L. Barra, X. Zhong, K. Park, R. Sessoli, *Phys. Chem. Chem. Phys.* **2014**, *16*, 17220–17230.

[52] D. Menozzi, E. Biavardi, C. Massera, F.-P. Schmidtchen, A. Cornia, E. Dalcanale, *Supramol. Chem.* **2010**, *22*, 768–775.

[53] B. Ballarin, G. A. Battiston, F. Benetollo, R. Gerbasi, M. Porchia, D. Favretto, P. Traldi,

Inorg. Chim. Acta **1994**, *217*, 71–78.

[54] A. Rodger, B. F. G. Johnson, *Inorg. Chem.* **1988**, *27*, 3061–3062.

[55] M. Barfield, B. Chakrabarti, *Chem. Rev.* **1969**, *69*, 757–778.

[56] A. I. Vogel, *Vogel's Textbook of Practical Organic Chemistry*, 5th ed., revised by B. S. Furniss, A. J. Hannaford, P. W. G. Smith, A. R. Tatchell, Longman Scientific & Technical, Harlow, UK, **1989**.

[57] G. R. Fulmer, A. J. M. Miller, N. H. Sherden, H. E. Gottlieb, A. Nudelman, B. M. Stoltz, J. E. Bercaw, K. I. Goldberg, *Organometallics* **2010**, *29*, 2176–2179.

[58] R. M. Lynden-Bell, R. K. Harris, *Nuclear Magnetic Resonance Spectroscopy*, Thomas Nelson & Sons Ltd, London, UK, **1969**.

[59] A. Altomare, G. Cascarano, C. Giacovazzo, A. Guagliardi, M. C. Burla, G. Polidori, M. Camalli, *J. Appl. Crystallogr.* **1994**, *27*, 435–435.

[60] G. M. Sheldrick, *Acta Crystallogr., Sect. C: Struct. Chem.* **2015**, *71*, 3–8.

[61] L. J. Farrugia, *J. Appl. Crystallogr.* **2012**, *45*, 849–854.

[62] A. Thorn, B. Dittrich, G. M. Sheldrick, *Acta Crystallogr., Sect. A: Found. Crystallogr.* **2012**, *68*, 448–451.

[63] Persistence of Vision Pty. Ltd., *Persistence of Vision Raytracer (Version 3.7) [Computer Software]*, Retrieved from http://www.povray.org/download/, **2021**.

[64] F. Neese, *Wiley Interdiscip. Rev.: Comput. Mol. Sci.* **2018**, *8*, e1327.

[65] V. Barone, M. Cossi, *J. Phys. Chem. A* **1998**, *102*, 1995–2001.

[66] J. P. Perdew, K. Burke, M. Ernzerhof, *Phys. Rev. Lett.* **1996**, *77*, 3865–3868.

[67] S. Grimme, S. Ehrlich, L. Goerigk, *J. Comput. Chem.* **2011**, *32*, 1456–1465.

[68] S. Grimme, J. Antony, S. Ehrlich, H. Krieg, *J. Chem. Phys.* **2010**, *132*, 154104.

[69] F. Weigend, R. Ahlrichs, *Phys. Chem. Chem. Phys.* **2005**, *7*, 3297–3305.

[70] P. J. Stephens, F. J. Devlin, C. F. Chabalowski, M. J. Frisch, *J. Phys. Chem.* **1994**, *98*, 11623–11627.

[71] A. D. Becke, *J. Chem. Phys.* **1993**, *98*, 5648–5652.

[72] F. Jensen, *J. Chem. Theory Comput.* **2015**, *11*, 132–138.

Table of contents

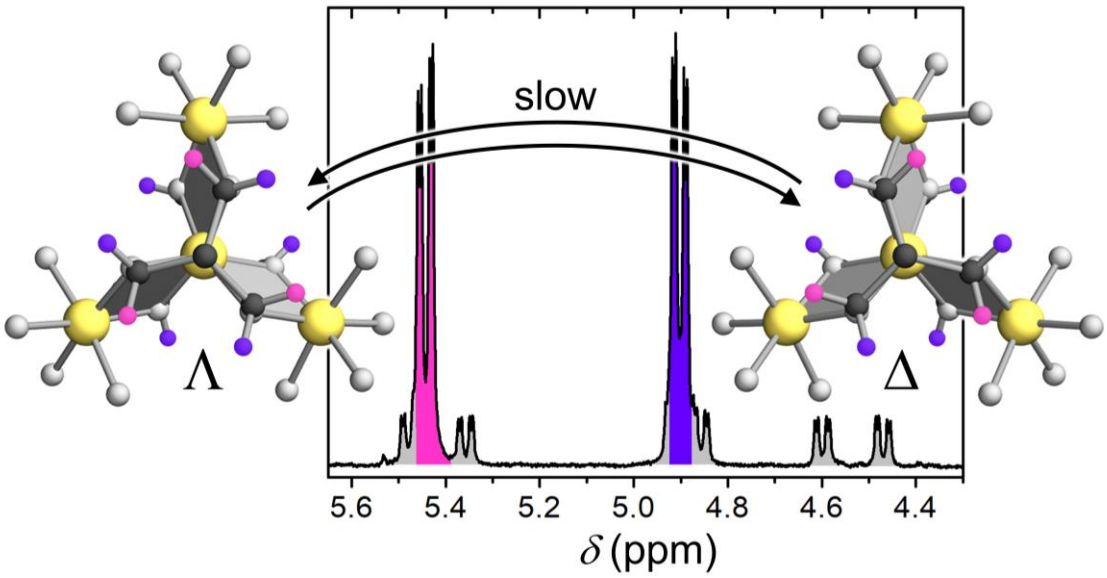

A chiral tetragallium(III) complex isostructural to the family of propeller-like $Fe^{III}_3M^{III}$ single-molecule magnets (M = Fe, Cr, V) was prepared and found to give spectacularly resolved NMR spectra in solution. We clearly identified two diastereoisomers with different symmetry in solution and used density functional theory calculations to demonstrate that their Λ and Δ optical antipodes interconvert slowly over NMR timescale.